

# Effect of Nuclei Concentration on Cavitation Cluster Dynamics

M. Arora,\* C.D. Ohl, and D. Lohse

*Department of Applied Physics,*

*Physics of Fluids,*

*University of Twente,*

*Postbus 217,*

*7500 AE Enschede,*

*The Netherlands.*

(Dated: July 2, 2007)

## Abstract

Cavitation cluster dynamics after the passage of a single pressure wave is studied for different concentrations of artificial cavitation nuclei (30 to  $3 \cdot 10^5$  nuclei/ml). With increasing concentration of cavitation nuclei the life time of the cavitation cluster is prolonged. Additionally, we find that the spatial extent of the cluster decreases with higher nuclei concentration. The experimental data for concentrations less than 400 nuclei/ml are compared to simulations with a Rayleigh-Plesset type equation, taking into account bubble-bubble interaction. For higher concentrations (more than 1000 nuclei/ml) the observed radial cluster dynamics is compared with an calculations from axisymmetric cavity-collapse model.

## I. INTRODUCTION

Cavitation bubbles often occur in ensembles or clusters. One of the methods to generate clusters of bubbles is to apply a single, intensive, pulsed pressure wave. In its tensile phase gaseous nuclei being present in the liquid explode and form a cavitation cluster. When the ambient pressure is restored, these cavitation bubbles undergo violent collapse. The destructive nature of cavitation clusters is widely reported in scientific literature, for example in hydrodynamics cavitation<sup>1-3</sup> and in shock wave lithotripsy<sup>4,5</sup>.

The interaction between the bubbles in a cavitation cluster is very complex<sup>6-10</sup>. In this article we want to address the applicability of simple models to predict the dynamics of the individual cavitation bubbles and/or the cavitation cluster over a wide range of the nuclei concentration (i.e. 30 to  $3 \cdot 10^5$  per ml). The work has been stimulated by the findings that the life-time of cavitation bubbles increases with higher bubble densities<sup>11-13</sup>. The analysis presented in this paper might be relevant to the field of shock wave lithotripsy where recent numerical works<sup>11,15</sup> emphasize the effect of nuclei concentration on the cluster dynamics. Additionally, clusters of cavitation bubbles are also of importance in sonochemistry<sup>16,17</sup>.

## II. CAVITATION CLUSTER EXPERIMENTS

A single pressure pulse is generated with a piezoelectric shock wave generator. It is a modified source from the commercial lithotripter Piezolith 3000 (Richard Wolf GmbH, Knittlingen, Germany). Details on the experimental setup and the acoustic source are available in Arora *et al.*<sup>12</sup> and Riedlinger *et al.*<sup>18</sup>, respectively.

In this study we use ultrasound contrast agent SonoVue (Bracco, Geneva, Switzerland) as cavitation nuclei. These consist of phospholipid shelled microbubbles with a mean diameter of  $2.5 \mu\text{m}$ . A stock suspension of contrast agent bubbles is prepared by mixing 5 ml water per vial contrast agent bottle ( $\approx 20\text{mg}$  of solids) as prescribed for medical usage.

---

\*Electronic address: [m.arora@tnw.utwente.nl](mailto:m.arora@tnw.utwente.nl)

The number density of bubbles is measured with a Neubauer cell-counting chamber under a microscope. Even though the naturally present nuclei (e.g. dirt particles) may have larger variations in size (and thus corresponding nucleation threshold), the usage of artificial nuclei allows us to have control on number density independent of tensile strength used. The desired concentrations of cavitation nuclei are obtained by preparing successive intermediate dilutions. Care is taken to ensure that the suspension is well mixed at each dilution step. For all the experiments, partially degassed (approx. 3 mg/l O<sub>2</sub> content, corresponding to 30% of saturation concentration) and de-inoized water is used.

The finally desired concentration of artificial cavitation nuclei is obtained by adding an appropriate amount of intermediate dilution to a non-seeded liquid in a bag around the acoustic focus of the shock wave generator. The bag is made from an acoustically and optically transparent bag made of low density polyethylene. It contains approximately 10 l of liquid with the desired concentration of cavitation nuclei.

Before the cavitation nuclei are added the pressure signal at the acoustic focus of the lithotripter is recorded with a fiber optic hydrophone (FOPH-500, RP Acoustics, Germany). Pressure measurements near to cavitation bubble clusters are hampered because the fragile fiber tip is easily damaged especially at higher nuclei concentrations.

Figure ?? shows a typical pressure recording in the absence of artificial nuclei. The pressure pulse consist of two phases: first a fast-rising compressive phase with a peak amplitude of 35 MPa lasting for 1.5  $\mu$ s. It is followed by a tensile phase with a peak amplitude of about -10 MPa lasting for approx. 3.5  $\mu$ s. This magnitude and duration of the tensile phase is sufficient to cause cavitation without artificial cavitation nuclei, see top left frame of Fig. ?. The cavitation bubbles around the focal region are well separated and they have a typical lifetime of  $150 \pm 10 \mu$ s. The lifetime of a bubble is defined as the time period between cavitation inception and the first collapse of the bubble. In the absence of artificial cavitation nuclei about 20 cavitation bubbles per ml are expanded in the focal region.

After adding artificial cavitation nuclei the shape of the second part of the pressure wave gets strongly modified, whereas the first part remains practically the same (see inset

Fig. ??). These effects are enhanced with increased concentration of cavitation bubbles. A similar finding has been reported recently by Liebler *et al.*<sup>15</sup>.

The dynamics of the cavitation cluster is recorded with a high speed CMOS-camera (ultima APX-RS Fastcam, Photron) at a framing rate of 50000 fps. The size of the images is  $384 \text{ pixel} \times 112 \text{ pixel}$  which correspond to a field of view of  $79 \text{ mm} \times 23 \text{ mm}$ . This gives an optical resolution of  $206 \mu\text{m}$  per pixel. Thus isolated bubbles with a radius of approx.  $200 \mu\text{m}$  can be resolved. The high-speed camera is triggered simultaneously with the shock wave generator and the scene is illuminated with diffuse back-illumination. The life-time of the cavitation clusters is determined by visual inspection of the recordings. Additionally, the width of sufficiently dense cavitation clusters are determined by digital image processing.

Figure ?? depicts the shape of the cavitation cluster at various concentrations of cavitation nuclei  $65\mu\text{s}$ ,  $165\mu\text{s}$  and  $265\mu\text{s}$  after the shock-front has passed the acoustic focus.

At low to moderate concentrations of the cavitation nuclei (37 to 370 nuclei/ml) individual bubbles larger than the optical resolution of the system can be identified. Beyond 1000 nuclei/ml it becomes increasingly difficult to separate individual bubbles from each other.

Interestingly, the life-time of the cavitation cluster increases from  $150 \mu\text{s}$  for the plain water case to  $350 \mu\text{s}$  for the highest concentration, see Fig. ?. In an attempt to model the cavitation cluster dynamics we distinguish between the case of sparsely populated bubble clusters, defined as a cluster of bubbles that do not grow to come close to each other, and the case of densely populated bubble cluster, in which the bubbles do come fairly close during the growth. For the first case (nuclei concentrations below 400 nuclei/ml) a modified spherical Rayleigh-Plesset equation is applied at the level of the individual bubble (section III), whereas in the second case an axisymmetric model for the volume dynamics of the dense cluster is employed (section IV).

### III. DYNAMICS OF SPARSELY POPULATED CLUSTERS

The Rayleigh-Plesset (RP) model describes the dynamics of single spherical bubbles. It is derived by integrating the momentum balance equation in radial direction assuming spherical symmetry<sup>19,20</sup>.

$$R\ddot{R} + \frac{3}{2}\dot{R}^2 = \frac{1}{\rho} \left( P_g + P_v - P(t) - P_0 - \frac{2\sigma}{R} - \frac{4\eta\dot{R}}{R} - \frac{R\dot{P}_g}{c_l} \right) \quad (1)$$

Here,  $R$  is the radius of the single cavity,  $P_0 = 1.013 \cdot 10^5 \text{Pa}$  is the constant atmospheric pressure,  $P(t)$  is the far-field driving sound pressure (shown in Fig. ??) and  $P_g$  the pressure inside the cavitation bubble, calculated assuming adiabatic gas law:

$$P_g = \left( P_0 + \frac{2\sigma}{R_0} - P_v \right) \left( \frac{R_0}{R} \right)^{3\gamma}. \quad (2)$$

The remaining physical parameters are density  $\rho = 1000 \text{kg}\cdot\text{m}^{-3}$ , coefficient of surface tension  $\sigma = 0.073 \text{kg}\cdot\text{s}^{-2}$ , water viscosity  $\eta = 1.00 \times 10^{-3} \text{Pa}\cdot\text{s}$  and sound velocity in water  $c_l = 1485 \text{m/s}$ . The last three terms in the brackets of Eq. 1 refer to the affect of surface tension, viscosity and sound emission from the bubble. Although we include these terms in the present analysis for completeness, they hardly effect the dynamics of the bubble. In a minimalistic model these terms also can be neglected. So far the model does not include the effect of neighboring bubbles.

To modify this equation to include bubble-bubble interaction an additional pressure term needs to be added. It can be derived from the summed velocity potential of neighboring bubbles<sup>10,21</sup>:

$$\phi = \left( \sum_i \frac{1}{r_i} \dot{R}_i R_i^2 \right), \quad (3)$$

where  $r_i$  is the distance to its  $i^{\text{th}}$  neighbor bubble with radii  $R_i$ . The higher order interaction terms, as often derived in the case of two bubbles<sup>22</sup>, can also be computed for multibubble systems<sup>9</sup> and but are neglected in this analysis. Further, we assume that locally all bubbles show the same radial dynamics, thus subscript  $i$  can be dropped from  $R_i$ . With the

assumption of a uniform number density of cavitation nuclei per unit volume,  $N$ , Eq. (3) can be rewritten as an integral in space:

$$\phi = R^2 \dot{R} \sum_i \frac{1}{r_i} \approx R^2 \dot{R} N \int_0^{\delta r} \frac{1}{r'} 4\pi r'^2 dr'. \quad (4)$$

Here,  $\delta r$  is the distance up to which bubble-bubble interactions are considered. We note that the integral, Eq. (4), grows unbounded for  $\delta r \rightarrow \infty$ . In reality the finite speed of sound and the acoustic shielding by bubbles prevent their mutual interaction at larger distances. Thus  $\delta r$  should be restricted to a finite distance. Here, we choose as a first approximation a concentration dependent cut-off distance of one average inter-bubble distance  $D_{mean}$ :

$$\delta r \equiv D_{mean} = \frac{1}{N^{1/3}}. \quad (5)$$

After adding the time derivative of Eq. (4) as an additional pressure term into the RP Eq. (1) we obtain

$$\alpha R \ddot{R} + \beta \dot{R}^2 = \frac{1}{\rho} \left( P_b - P(t) - P_0 - \frac{2\sigma}{R} - \frac{4\eta \dot{R}}{R} - \frac{R \dot{P}_g}{c_l} \right), \quad (6)$$

where  $\alpha = (1 + 2\pi R N^{1/3})$  and  $\beta = (\frac{3}{2} + 4\pi R N^{1/3})$ .

Please, note that when  $N \rightarrow 0$ , the original RP equation is obtained. With modified RP Eq. (6) we calculate the change in the radial dynamics of the bubbles and their collapse time for various nuclei concentrations. Figure ?? compares the radial dynamics of a single bubble with an initial size of  $1\mu\text{m}$  being driven by a single pressure pulse for  $N=0, 1$  and  $100$  nuclei/ml. The driving pressure pulse used in all the above cases is the measured pressure pulse (with no artificial nuclei) as shown in fig. ?. The graph shows that the bubble life time is increased and its maximum size is reduced at increasing densities of cavitation nuclei. In fig. ?? the collapse time as a function of nucleus concentration is plotted as a dashed line and it is compared with experimental measurements (vertical error bars).

In agreement with the observation, the model predicts an increase in the bubble life time of  $50\mu\text{s}$  when the concentration is increased from  $40$  nuclei/ml to  $\approx 400$  nuclei/ml. Although

the predictions are within the measured error limits, it should be noted that the recorded pressure pulse used for the driving far-field pressure,  $P(t)$ , in Eq. (6) is already affected by the presence of nearby bubbles. Therefore, the agreement of the absolute collapse time should be taken with some caution. It has been found that the peaks following the tensile phase as depicted in Fig. ?? do alter the absolute collapse time.

At higher concentrations the bubbles very close to each other and the model becomes inapplicable. Therefore, in order to capture the cloud dynamics at higher number densities we make use of a different model which describes the cluster as a single cylindrical void.

#### IV. DYNAMICS OF DENSELY POPULATED CLUSTERS

For number densities above 1000 bubbles/ml the cluster looks quite different, see Fig. ??: The shape of the cluster becomes more homogeneous and it is separated from the surrounding liquid by a sharp boundary. The collapse of the cluster proceeds progressively from the cluster boundary toward its center. These observations suggest to model the shrinkage of the cluster boundary as a shock front. The speed,  $\dot{X}$ , at which the cluster collapses is identified with the propagation speed of the shock front<sup>23,24</sup> which is given by:

$$\dot{X} = \left( \frac{P_1}{\rho\beta(1-\beta)} \right)^{1/2}. \quad (7)$$

Here,  $P_1$  is the pressure just outside the cavitation cluster driving the collapse, and  $\beta$  the void fraction within the cluster. In the case of a cavitation cluster with well separated spherical bubbles  $\beta$  is given by  $N \cdot \frac{4}{3}\pi R^3$ , which in general is a time varying quantity. However, when the bubbles grow those inside the cluster become increasingly shielded from the outside pressure field and for large  $N$ , and we can assume that inside the cluster  $\beta$  reaches a constant value. Note that, for large enough void fractions,  $\beta > 0.1$ , the time required to collapse individual bubbles is of the same order of magnitude as that for the passage of shock front over the bubble  $\sim R\sqrt{\frac{\rho}{P_1}}$ , further justifying identification of the speed of the cluster collapse with the speed of the shock front.

The pressure  $P_1$  just outside the cylindrical cluster is coupled with the far field pressure

$P_0$  far away by a momentum balance in cylindrical coordinates. As derived by Hansson and Mørch<sup>23</sup>, the motion of the cluster boundary  $X$  can be modelled with a second order ODE:

$$(X\ddot{X} + \dot{X}^2)\ln \frac{x_c}{X} - \dot{X}^2 + \frac{\beta}{2}\dot{X}^2 \left[ \left( \frac{X}{x_c} \right)^2 + 1 \right] = -\frac{1}{\rho\beta}P_0 \quad . \quad (8)$$

Here  $x_c$  is the typical size scale of the experimental setup, in our case  $x_c = 0.2$  m, is approximately the radius of the liquid compartment. For the limiting case of  $\beta = 1$ , the above equation becomes the the void collapse equation in cylindrical geometry<sup>25,26</sup>(2D-Rayleigh equation).

Figure ?? compares the experimentally measured diameter of the cavitation cluster with Eq. (8) for a cavitation nuclei density of a)  $3 \cdot 10^5$  bubbles/ml and b)  $3.7 \cdot 10^3$  bubbles/ml. As there is no simple experimental means for measuring the void fraction  $\beta$ , the model calculations have been fitted to the experimental collapse time by choosing  $\beta = 0.34$  and  $0.22$  respectively. Thus, we find that increase of the number of cavitation nuclei leads to an increase of the maximum value of  $\beta$ , but shielding limits the growth of the bubbles, and thus the effect of increasing  $N$ .

It is interesting to note, that the maximum bubble radius can be estimated from the best fit value of the void fraction. We find for  $\beta = 0.34$  and  $\beta = 0.22$  with the respective number densities a bubble radius  $R$  of  $0.06$  mm and  $0.24$  mm, respectively. Although, the optical resolution of  $0.2$  mm/pixel does not allow a direct measurement of the bubble radius, individual bubbles can be identified in Fig. ??b, whereas it can not be done for the  $\beta = 0.34$  case, see Fig. ??a.

## V. CONCLUSION

The dynamics of cavitation clusters is strongly modified when artificial cavitation nuclei are added. With increasing concentration of nuclei we find a prolongation of the lifetime and a decrease in the maximum bubble size. Two regimes of cluster dynamics are considered: With nuclei number densities below  $400$  bubbles/ml sparsely populated clusters with fuzzy

boundaries are developed. For these, the presented modified RP equation including nearest neighbor interaction terms seems to give a sufficient description of the bubble dynamics at the center of the cluster. Tanguay and Colonius<sup>11</sup> in their numerical simulations also find increase in lifetime of bubbles but also an increase in the maximum size of the bubbles with increasing void fraction. Even though the model for the sparse cluster presented in this work agrees with the experimental results it is subject to further verification. Of interest might be experiments which record the bubble size and the void fraction independently as function of time. In the second regime, i.e. for bubble densities of 1000 nuclei/ml and above it becomes more appropriate to model the cluster as a single entity having a constant void fraction. Here, very high void fractions in the range of 20-35% agree with collapse dynamics. Yet, to increase confidence into these models further experiments with other pressure sources should be conducted to evaluate the robustness of the rather simple models.

The range of cavitation nucleus densities examined in this study extends much beyond the range in which single bubble models are applicable. Real life nucleation conditions are likely to generate sparsely populated as well as densely populated bubble clusters. For example, in lithotripsy sparsely populated clusters may arise from natural nuclei present *in-vivo* or *in-vitro*, while densely populated clusters require accumulation of extra nuclei. Such extra nuclei may come from fragmentation of stone pieces, or may be gaseous remains of cavitation bubbles from previous shots<sup>12</sup>. Similarly, cavity clusters are likely to be created in high intensity ultrasonic equipment such as ultrasonic cleaners, sono-chemical reactors, etc., depending only on the number of cavitation nuclei being present in the active region of the device.

The absolute values of the nucleus densities characteristic of the two regimes defined in this paper will vary in dependence of the parameters of tensile phase, such as its pulse strength and duration, properties of the liquid in which cavitation is taking place, etc..

The funding of the work by FOM and NWO (both The Netherlands) is acknowledged. We are very thankful to Knud Aage Mørch and Andrea Prosperetti for various insightful discussions and refining the manuscript. We are also grateful to Marko Liebler (University

of Karlsruhe) for illuminating us on wave propagation at higher nuclei densities.

## References

- <sup>1</sup> G.E. Reisman, Y.C. Wang, and C.E. Brennen, “Observations of shock waves in cloud cavitation,” *J. Fluid Mech.* **355**, 255-283 (1998).
- <sup>2</sup> G. Kuiper, “Cavitation research and ship propeller design”, *Applied Scientific Research*,**58**, 33-50 (1998).
- <sup>3</sup> C.E. Brennen, *Cavitation and Bubble Dynamics* (Oxford Univ. Press, 1995).
- <sup>4</sup> O.A. Sapozhnikov, V.A. Khokhlova, M.R. Bailey, and L.A. Crum, “Effect of overpressure and pulse repetition frequency on cavitation in shock wave lithotripsy,” *J. Acoust. Soc. Am.* **112**, 1183-1195 (2002).
- <sup>5</sup> Y. Matsumoto, J.S. Allen, S. Yoshizawa, T. Ikeda, and Y. Kaneko, “Medical ultrasound with microbubbles,” *Exp. Therm. Fluid Sci.* **29**, 225-265 (2005).
- <sup>6</sup> L. van Wijngaarden, “On equations of motion for mixtures of liquid and gas bubbles,” *J. Fluid Mech.* **33**, 465-474 (1968).
- <sup>7</sup> D.Z. Zhang and A. Prosperetti, “Averaged equations for inviscid disperse two-phase flow,” *J. Fluid Mech.* **267**,185219 (1994).
- <sup>8</sup> Y.C. Wang and C.E. Brennen, “Numerical computation of shock waves in a spherical cloud of cavitation bubbles,” *J. Fluids Eng. Trans. ASME* **121**, 872-880 (1999).
- <sup>9</sup> G.L. Chahine, “Pressure generated by a bubble cloud collapse,” *Chem. Eng. Commun.* **28**, 355-367 (1983).
- <sup>10</sup> G.L. Chahine, and H. L. Liu , “A Singular Perturbation Theory of the Growth of a Bubble Cluster in a Superheated Liquid”, *J. Fluid Mech.*, **156**, 257-279, 1985.
- <sup>11</sup> M. Tanguay and T. Colonius, “Progress in Modeling and Simulation of Shockwave Lithotripsy (SWL),” in *Fifth International Symposium on Cavitation (CAV2003)*, 1-4 November 2003, Osaka, Japan.
- <sup>12</sup> M. Arora, L. Junge, and C.D. Ohl, “Cavitation cluster dynamics in shock-wave

- lithotripsy: Part 1. Free field,” *Ultrasound Med. Biol.*, **31**, 827-839 (2005).
- <sup>13</sup> N. Bremond, M. Arora, S. Dammer, C.D. Ohl, and D. Lohse, “Bubble nucleation on surfaces”, *J. Phys.: Condens. Matter*, **17** S3603-S3608 (2005).
- <sup>14</sup> Y. C. Wang, “Effects of nuclei size distribution on the dynamics of a spherical cloud of cavitation bubbles”, *J. Fluids Eng. Trans. ASME* **121**, 881-886 (1999)
- <sup>15</sup> M. Liebler, T. Dreyer, R.E. Riedlinger, “Nonlinear Modelling of Interactions between Ultrasound and Cavitation Bubbles”, *Acta Acustica*, 2006(in press).
- <sup>16</sup> K.S. Suslick, “Sonochemistry”, *Science*, **247**, 1439-1445 (1990).
- <sup>17</sup> P.M. Kanthale, P.R. Gogate, A.B. Pandit, and A.M. Wilhelm, “Dynamics of cavitation bubbles and design of a hydrodynamic cavitation reactor: cluster approach”, *Ultrasonics Sonochemistry*, **12**, 441-452 (2005).
- <sup>18</sup> R. Riedlinger, T. Dreyer, and W. Krauss, “Small aperture piezo sources for lithotripsy,” In *Proc. 17th Int. Congress on Acoustics*. vol 4 ed A Bettucci, 2001, Rome, Italy.
- <sup>19</sup> Rayleigh, Lord. “On the pressure developed in a liquid during the collapse of a spherical cavity”, *Phil. Mag.*, **34**, 94-98 (1917).
- <sup>20</sup> M.S. Plesset, and A. Prosperetti, “Bubble dynamics and cavitation”, *Ann. Rev. Fluid Mech.*, **9**, 145-185 (1977).
- <sup>21</sup> A. Kubota, H. Kota, H. Yamaguchi, “A New Modeling of Cavitating Flows - A Numerical Study of Unsteady Cavitation on a Hydrofoil section”, *J. Fluid Mech.*, **240**, 59-96 (2002).
- <sup>22</sup> A. Harkin, T.J. Kaper, A. Nadim, “Coupled pulsation and translation of two gas bubbles in a liquid”, *J. Fluid Mech.*, **445**, 377-411 (2001).
- <sup>23</sup> I. Hansson and K.A. Mørch, “The Dynamics of Cavity Clusters in Ultrasonic (Vibratory) Cavitation Erosion”, *J. Appl. Phys.*, **51**, 4651-4658 (1980).
- <sup>24</sup> K.A. Mørch, “On Cavity Cluster Formation in a Focused Acoustic Field”, *J. Fluid Mech.*, **201**, 57-76 (1989).
- <sup>25</sup> H. N. Oguz and A. Prosperetti, “Dynamics of Bubble-Growth and detachment from a needle”, *J. Fluid Mech.*, **257**, 111-145 (1993).
- <sup>26</sup> D. Lohse, R. Bergmann, R. Mikkelsen, C. Zeilstra, D. van der Meer, M. Versluis, K. van

der Weele, M. van der Hoef, and H. Kuipers, “Impact on soft sand: Void collapse and jet formation”, *Phys. Rev. Lett.*, **93**, 198003 (2004).

## List of Figures

FIG. 1	A typical pressure recording at the focus of the lithotripter in the absence of artificial cavitation nuclei. The inset demonstrates the effect of addition of cavitation nuclei on the pressure wave at the focus. With increasing numbers of cavitation nuclei (indicated by direction the of the arrow) the duration of the tensile phase decreases and a secondary positive pressure pulse emerges. The primary pressure peak remains almost unaffected. . . . .	15
FIG. 2	Cavitation bubble clusters at three different times after the passage of the shock wave as obtained with various initial cavitation nuclei concentration, as stated at each row. The top row (control) corresponds to the case of plain water. The size of each frame is 79 mm × 23 mm. . . . .	16
FIG. 3	Radius-Time curve for individual bubbles at different nucleus concentrations when driven the pressure pulse in fig. reffig:pressure. The solid line corresponds to the case of very low nucleus density, $N \rightarrow 0$ , where as the dashed and dotted lines correspond to 1 and 100 bubbles/ml respectively. . . . .	17
FIG. 4	The collapse times of the cavitation cluster at varying nucleus concentrations driven by the pressure pulse in fig. reffig:pressure. The dashed line shows the result of numerical model taking into account bubble bubble interactions from neighboring bubbles in case of sparsely populated clusters. . . . .	18
FIG. 5	Evolution of the width of the cavitation cluster at two nucleus concentrations, a) $3.0 \cdot 10^5 ml^{-1}$ and b) $3.7 \cdot 10^3 ml^{-1}$ . These are compared with model for densely populated clusters, see Eq.(8)(solid line) by choosing appropriate values of $\beta$ . Selected frames at the indicated time are presented to demonstrate the cylindrical shape in both cases. . . . .	19

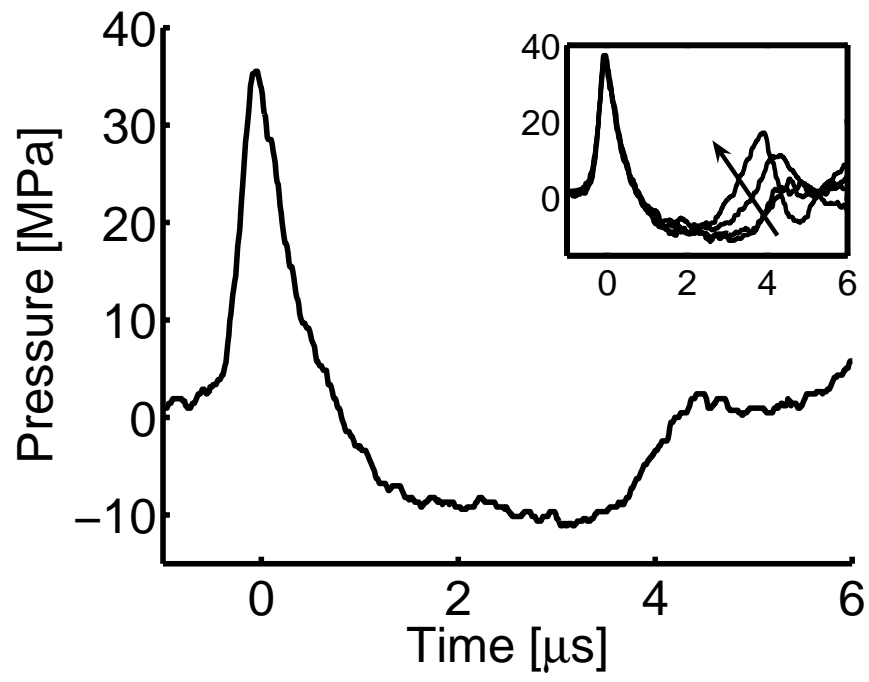


FIG. 1.

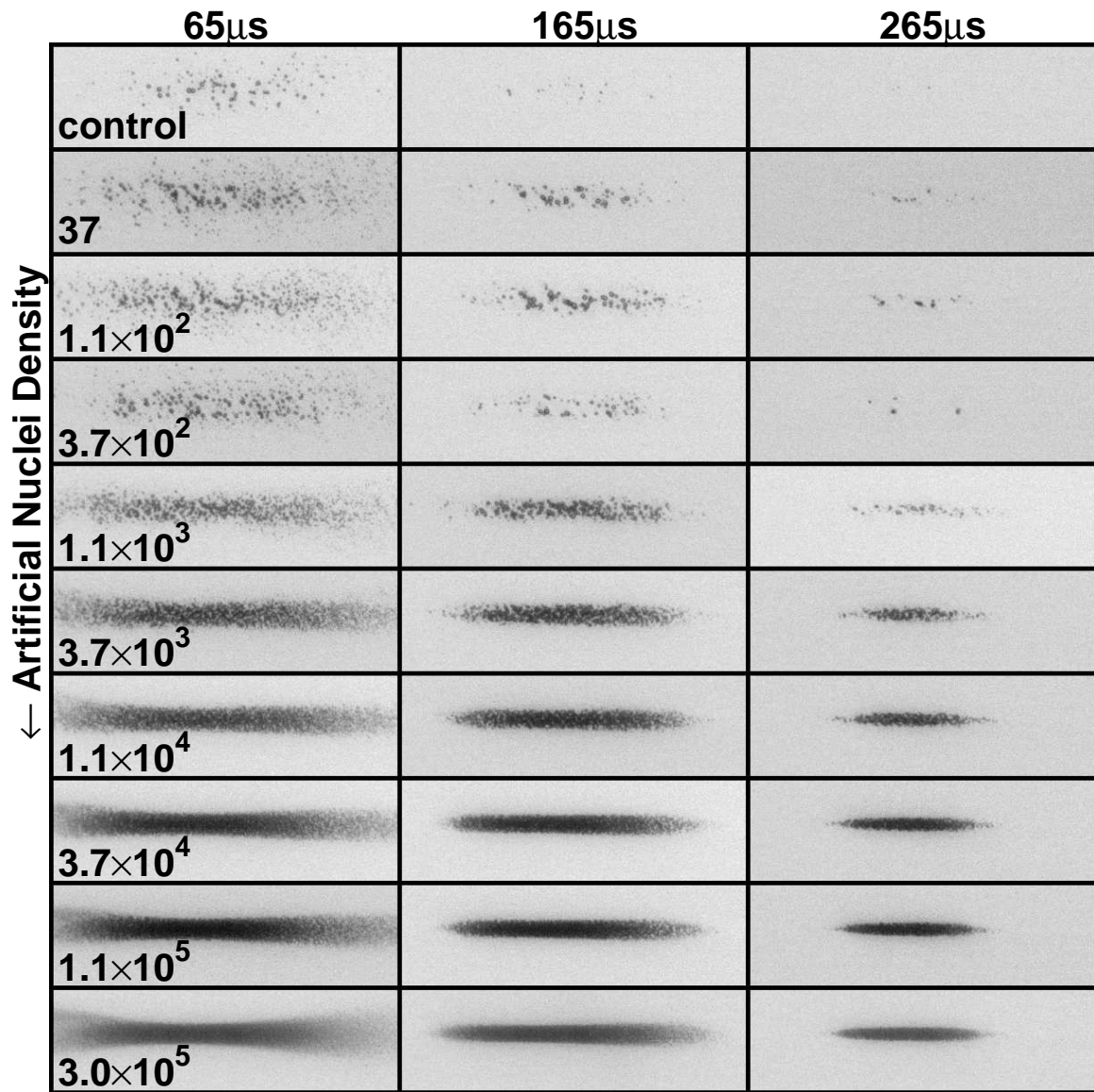


FIG. 2.

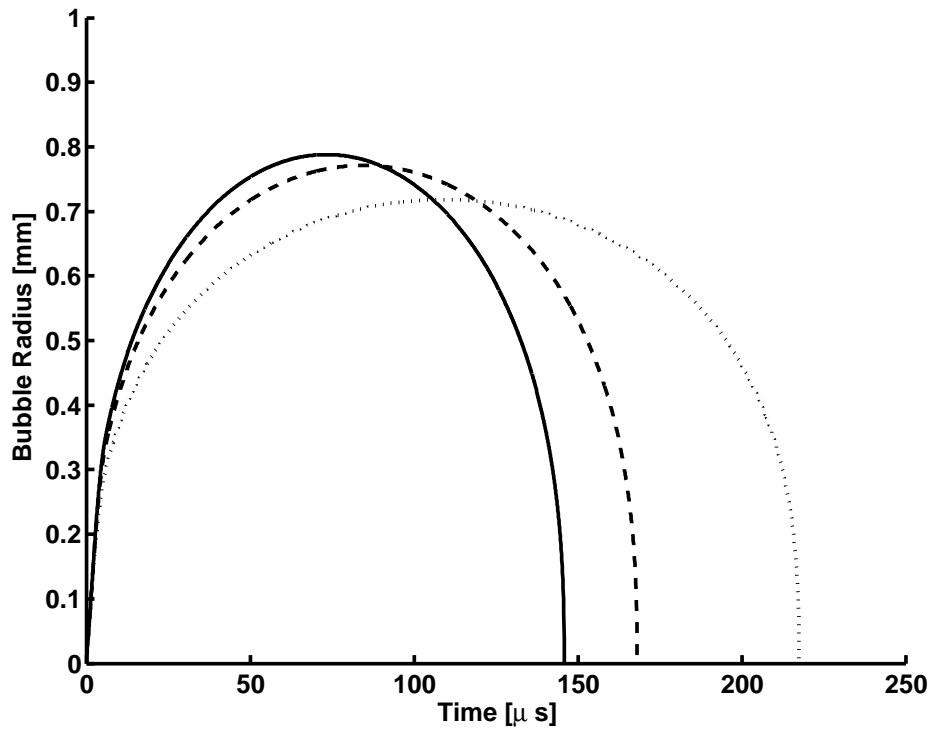


FIG. 3.

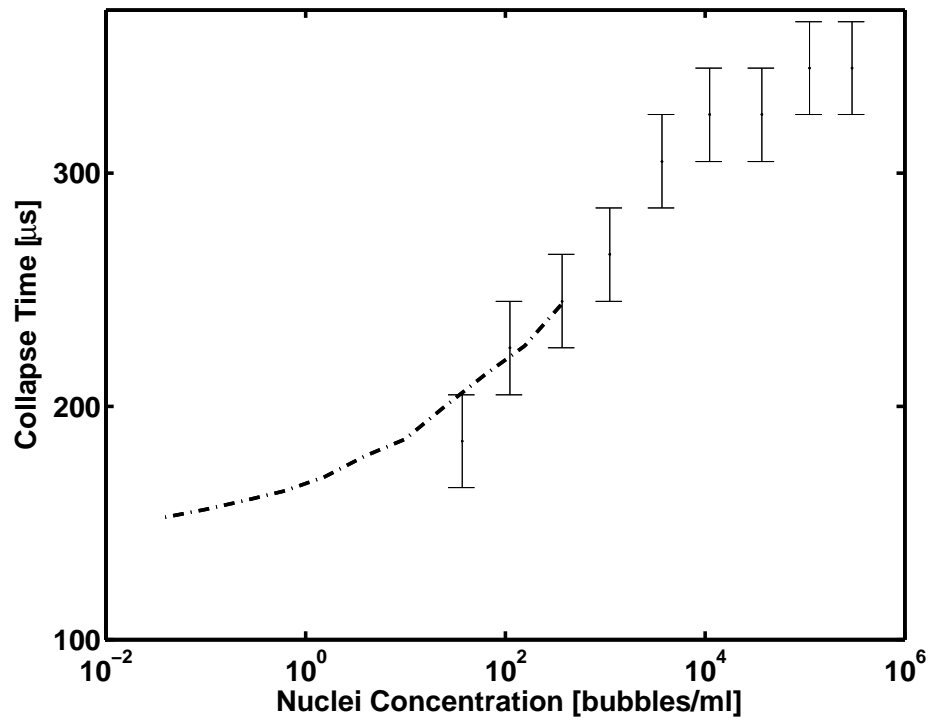
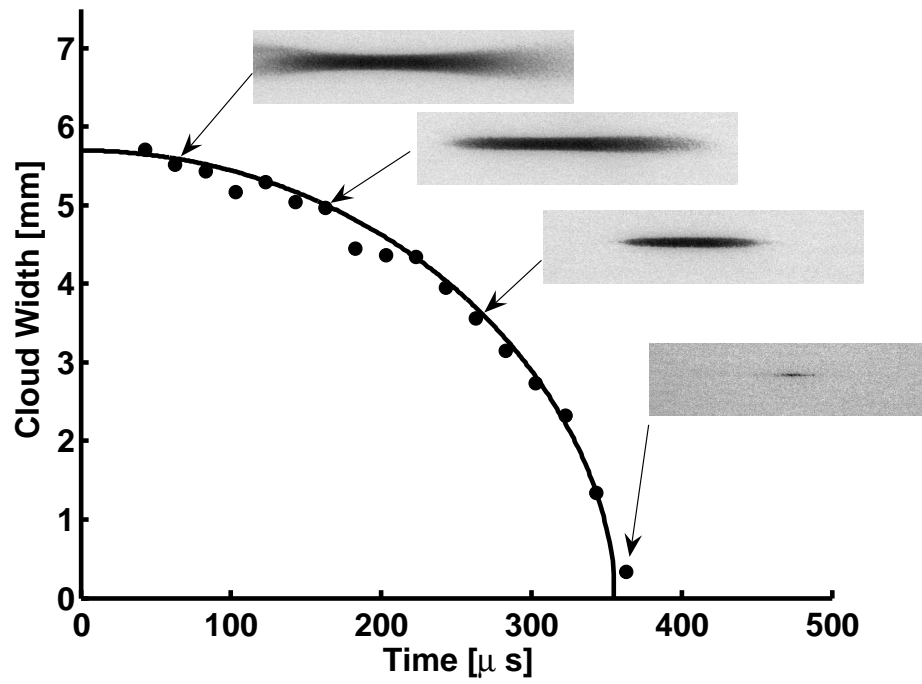
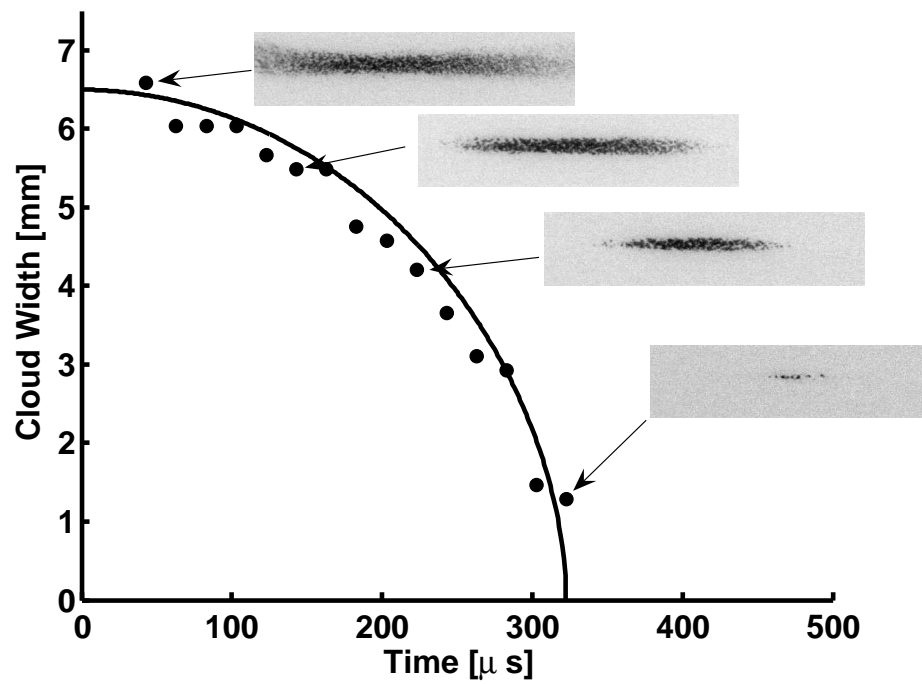


FIG. 4.



a)



b)

FIG. 5.